Chemical Research in Toxicology

Article

pubs.acs.org/crt

Electron and Spin-Density Analysis of Tirapazamine Reduction Chemistry

Jian Yin,[†] Rainer Glaser,*[,†] and Kent S. Gates*[,†,‡]

Departments of [†]Chemistry and [‡]Biochemistry, University of Missouri, Columbia, Missouri 65211, United States

Supporting Information

ABSTRACT: Tirapazamine (TPZ, **1**, 3-amino-1,2,4-benzotriazine 1,4-*N*,*N*-dioxide), the radical anion **2** formed by one-electron reduction of **1**, and neutral radicals **3** and **4** formed by protonation of **2** at O(N4) or O(N1), respectively, and their N−OH homolyses **3** → **5** + ·OH and **4** → **6** + ·OH have been studied with configuration interaction theory, perturbation theory, and density functional theory. A comprehensive comparative analysis is presented of structures and electronic structures and with focus on the development of an understanding of the spin-density distributions of the radical species. The skeletons of radicals **3** and **4** are distinctly nonplanar, several stereoisomeric structures are discussed, and there exists an intrinsic preference for **3** over **4**. The *N*-oxides **1**, **5**, and **6** have closed-shell singlet ground states and low-lying, singlet biradical (**SP-1**, **SP-6**) or biradicaloid (**SP-5**) excited states. The doublet radicals **2**, **3**, and **4** are heavily spin-polarized. Most of the spin density of the doublet radicals **2**, **3**, and **4** is located in one (N,O)-region, and in particular, **3** and **4** are not C3-centered radicals. Significant amounts of spin density occur in both rings in the singlet biradical(oid) excited states of **1**, **5**, and **6**. The dipole moment of the N2−C3(X) bond is large, and the nature of X provides a powerful handle to modulate the N2−C3 bond polarity with opposite effects on the two NO regions. Our studies show very low proton affinities of radical anion **2** and suggest that the pK_a of radical [**2**+H] might be lower than 6. Implications are discussed regarding the formation of hydroxyl from **3** and/or **4**, regarding the ability of **5** and **6** to react with carbon-centered radicals in a manner that ultimately leads to oxygen transfer, and regarding the interpretation of the EPR spectra of reduced TPZ species and of their spin-trap adducts.

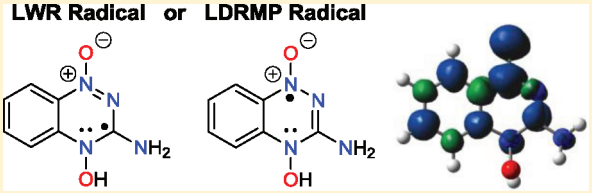

INTRODUCTION

Tirapazamine (TPZ, **1**, 3-amino-1,2,4-benzotriazine 1,4-*N*-dioxide) damages the DNA of solid tumor cells under hypoxic conditions.[1] It is generally agreed that once inside these cells, one-electron reduction of TPZ leads to highly oxidizing radical species, which can mediate the damage to the sugar−phosphate backbone and heterocyclic base residues of DNA. The mechanism of TPZ-mediated DNA strand cleavage has been studied extensively using experimental and theoretical approaches by the groups of Laderoute,[2−5] Lloyd,[6] Patterson,[7] Gates,[8−15] Anderson,[16−18] and Li,[19] and several mechanistic proposals have been advanced concerning the identities of the toxicologically active species and their formations.

In normally oxygenated cells, the primary TPZ metabolite **2** (3-amino-1,2,4-benzotriazine 1,4-*N*-dioxide anion) is rapidly oxidized back to **1**. The radical anion **2** has been detected by EPR spectroscopy, and the analyses by Lloyd et al.[6] and by Anderson et al.[18] both agree that the radical is mostly located in the (N1,O) region. In the hypoxic environment of solid tumors, the anion radical **2** has a longer lifetime and can be protonated at one of its two oxygen sites to form the neutral isomeric radicals **3** and/or **4**, respectively.[2,4,5] Laderoute, Wardman, and Rauth considered the C3-centered radical to be most important (LWR radical) based on semiempirical computations,[2] whereas Lloyd et al. argued in support of the N-centered nitroxide radical (LDRMB radical).[6] There exists no spectroscopic evidence of **3** or **4** in solution, and these protonated derivatives of **2** have only been discussed as the (activated) substrates for the reactions with spin traps. Subsequent N−OH bond homolysis of **3** and/or **4** then can lead to the release of hydroxyl radical,[8,13,14] a well-known DNA damaging agent.[20] Patterson and Taiwo detected the hydroxyl adduct of the spin-trap DMPO (5,5-dimethyl-1-pyrroline *N*-oxide) indicative of ·OH formation under these conditions.[7] A carbon centered-radical DMPO-R also was detected, but it was unclear whether this radical was formed by the addition of DMPO to **3**, **4**, or other species (i.e., DMSO or the DMSO-derived methyl radical).[7] Li et al. studied the relative stabilities of **3** and **4** and reported a preference for isomer **4** at B3LYP/6-31G* and B3LYP/6-311+G* in gas phase, but a marked preference for isomer **3** when aqueous solvation was considered via continuum methods. The ·OH loss from **3** and/or **4**, respectively, leads to the formation of isomers **5** and/or **6** of neutral, closed-shell 3-amino-1,2,4-benzotriazine monoxide, and isomers **5** and **6** have been identified in previous studies.[10,21] Li et al.[19] calculated the pathways for hydroxyl radical release, and at the B3LYP/6-31G(d) level the activation barriers for the reactions **3** → **5** + ·OH and **4** → **6** + ·OH, respectively, were reported as ΔH_0 = 5.0 and ΔH_0 = 15.6 kcal/mol, respectively.[19]

Received: December 14, 2011
Published: March 5, 2012

Scheme 1. Proposed Mechanisms for TPZ Activation

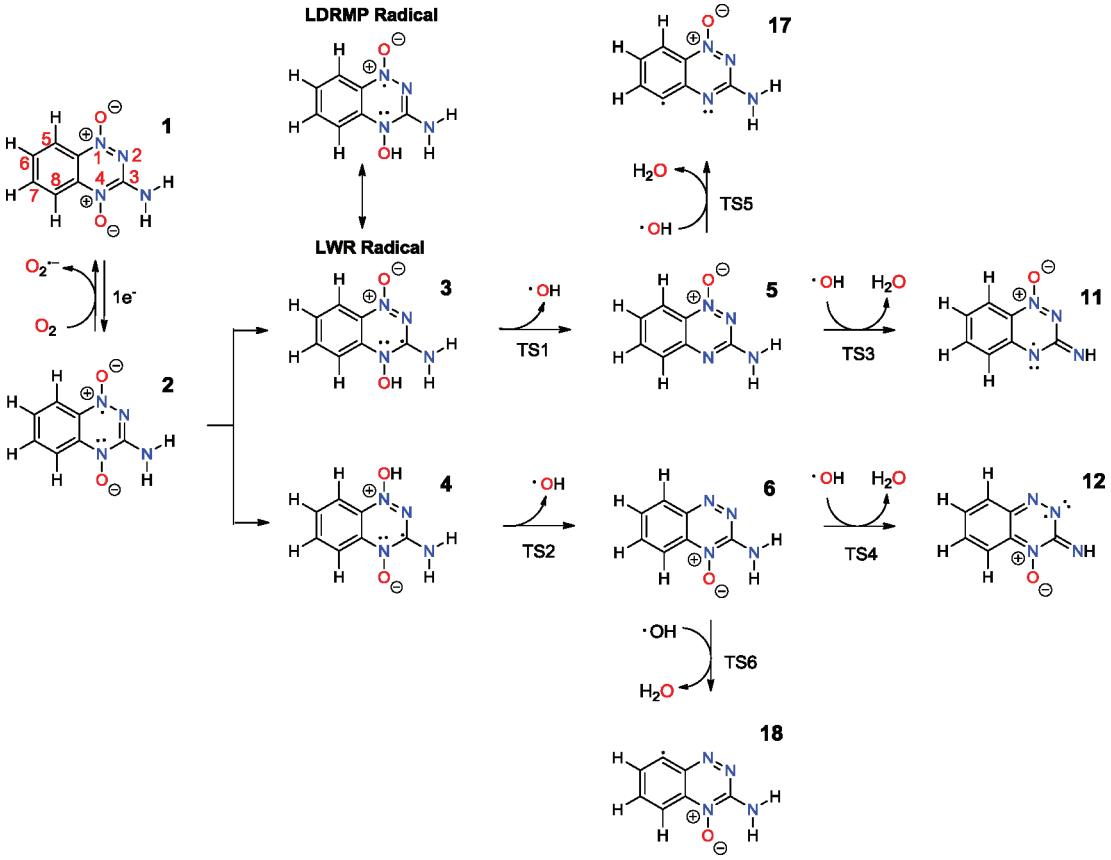

As an alternative to simple N−OH homolysis, Anderson and co-workers recently discussed the concerted dehydration of **3**, which may lead to the benzotriazinyl radical **11** (BTZ)[17] and/or the aryl radical **17**.[17,18] The analogous dehydration of isomer **4** would lead to radicals **12** and **18**, and these options also are included in Scheme 1. It is our premise that there may not be a fundamental difference between the mechanistic proposals of N−OH homolysis and dehydration and, instead, that the outcomes might depend on the chemistry after homolysis of **3** and/or **4**. Dehydration may be the result of a two-step reaction sequence that involves unimolecular N−OH homolysis and subsequent H-abstraction by ·OH. One should keep in mind that the observation of dehydration in the presence of a spin trap does not imply that the radicals produced by dehydration are involved in the medicinal activity of TPZ and its analogues.

We have explored the chemistry outlined in Scheme 1 with theoretical methods (density functional theory, perturbation theory, and configuration interaction theory) and with focus on the development of an understanding of the spin-density distributions of the radical species involved. In the present article, we report on the electronic structure of **1**, the reduction of **1** to **2**, the protonation of **2** to isomers **3** and **4**, and the N−OH homolyses **3** → **5** + OH and **4** → **6** + OH. A theoretical study of the stepwise dehydration is the subject of the companion article.[22] Theoretical studies of open-shell systems remain nontrivial, and π-radicals present significant computational and conceptual challenges because of spin delocalization and spin polarization. The proper assessment of the adequacies of the theoretical methods employed becomes especially important considering that spin polarization intrinsically is an effect of electron correlation. Hence, we present a discussion of concepts about spin-density distributions following our description of the theoretical methods. We can then tackle the discussion of the TPZ chemistry well equipped to recognize and resolve a number of apparent conflicts in the published literature and to draw conclusions with the requisite confidence and rigor.

COMPUTATIONAL METHODS

Calculations were carried out using the Gaussian 09 program[23] on a 64-processer SGI Altix system and a multivendor compute cluster with 170 compute nodes (Dell, IBM, ACT) and over 1000 Intel 64 Xeon processor cores.

The structures of neutral and charged species were optimized with the hybrid density functional method B3LYP[24] and with second-order Møller−Plesset perturbation theory (MP2),[25] and in conjunction with the 6-31G* basis set. Molecular models of the B3LYP/6-31G* optimized structures are shown in the Figures. The MP2/6-31G* structures look the same to the eye, and noticeable differences will be discussed. Harmonic vibrational analyses were performed for all stationary structures at both levels and employed to compute vibrational zero-point energies (VZPE), thermal energies (TE), and molecular entropies (S).

In the potential energy surface analyses, restricted wave functions were employed for closed shell systems (RB3LYP and RMP2), and unrestricted theory was employed (UB3LYP and UMP2) for open-shell systems. The results obtained at the B3LYP/6-31G* and MP2(full)/6-31G* levels are listed in Tables S1 and S2, respectively, in Supporting Information. Molecular models of the B3LYP/6-31G* optimized structures are shown in Figure 1, and the relative and activation energies computed at the B3LYP/6-31G* and MP2(full)/6-31G* levels, respectively, are reported in Tables 1 and 2, respectively. The reported data include energies ΔE, enthalpies at 0 K ($\Delta H = \Delta E +$

dx.doi.org/10.1021/tx2005458 | Chem. Res. Toxicol. 2012, 25, 620−633

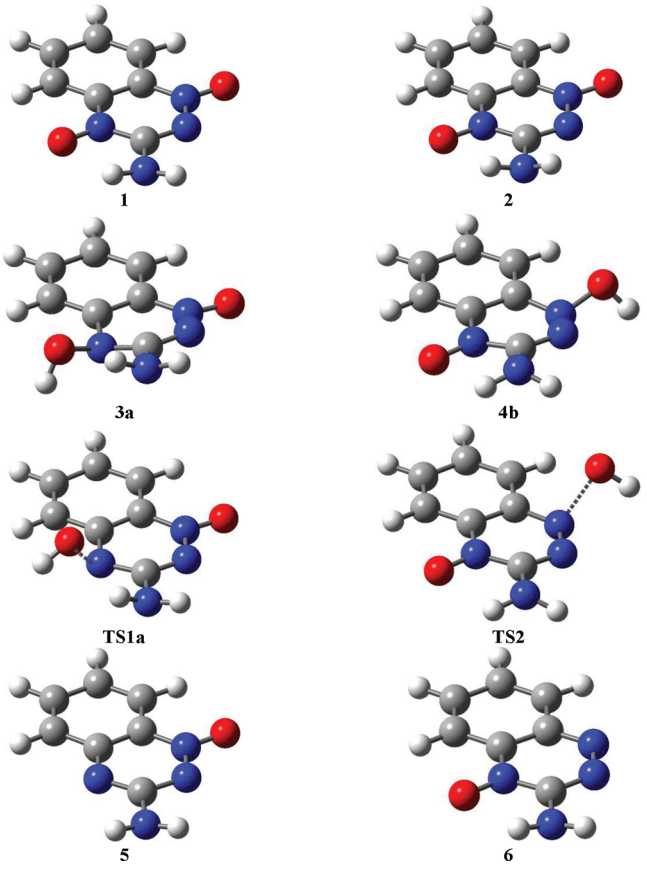

Figure 1. Tirapazamine (TPZ, **1**), the radical anion **2**, and isomers **3** and **4** of the radical resulting by O-protonation and products **5** and **6** formed by OH loss from isomers **3** and **4**. The B3LYP/6-31G* structures are shown.

$\Delta VZPE$) and 298 K ($\Delta H_{298} = \Delta E + \Delta TE$), and free enthalpies ($\Delta G_{298} = \Delta H_{298} - T{\cdot}\Delta S$).

We also performed single-point energy calculations with the configuration interaction method QCISD[26] using the same basis set and the B3LYP and MP2 optimized geometries, respectively. The total energies are included in Tables S1 and S2 (Supporting Information), and Tables 1 and 2 contain $\Delta E'$ and $\Delta G'$ values computed with the QCISD energies. The $\Delta G'$ values include the thermochemical corrections computed at the level of optimization, that is, $\Delta G' = \Delta E' + (\Delta G - \Delta E)$.

In some cases, the use of unrestricted wave functions gave stable spin-polarized wave functions for singlet systems (vide infra). The UQCISD energies of these spin-polarized excited states are listed in footnotes to Table S2 (Supporting Information), and RQCISD energies are provided for all singlet states in the QCI columns of Tables S1 and S2 (Supporting Information).

RESULTS AND DISCUSSION

Concepts about Electron and Spin-Density Distributions. *Spin Delocalization and Spin Polarization.* Unrestricted wave functions allow each electron to occupy its very own molecular orbital. It is important to realize that not just the "unpaired" electron in the Lewis structure of a radical will have its very own molecular orbital but that the α and β electrons of every "electron pair" in the Lewis structure each will have its very own molecular orbital. In many cases, the molecular orbitals of the α and β electrons of an "electron pair" are quite similar, and the electrons remain "effectively spin paired." However, the α and β electrons of an "electron pair" may adopt significantly different molecular orbitals, and the result is a spin-polarized electron pair: there will be regions with more α-spin density and other regions with more β-spin density. Spin polarization becomes important in radicals because the unpaired electron creates (at least) one center of α-spin density. This concentration of α-spin density will tend to spin-polarize proximate electron pairs such that their α electrons are on average closer to the center of α-spin density. The methyl radical is a well-known example where the unpaired π_α electron spin-polarizes the three CH bonds such as to increase the α-spin density at C while creating β-spin density at the hydrogens.[27] If the unpaired electron occupies a delocalized molecular orbital, then several centers of α-spin density are caused by the one unpaired electron. The spin density at each center will tend to spin-polarize proximate electron pairs such that the α-spin density at the centers are increased on average. The benzyl radical is a well-known example where the unpaired π_α electron occupies a delocalized MO, and spin-polarization occurs throughout the molecule.[28] The effects of spin delocalization and spin polarization often are complicated,[29] and it becomes impossible to understand the electronic structure with the simplistic idea that the MO of one unpaired electron would describe the spin density of the open-shell molecule. In general, therefore, one needs to discuss the spin density distribution of the molecule, that is, the difference between the electron density distributions of all α and all β electrons; $\rho^S = \rho^\alpha - \rho^\beta$. The spin-density distribution function ρ^S provides a practical connection to chemical reactivity because the system's radical reactivity tends to occur at positions with high α-spin concentration.

The electron density distributions $\rho = \rho^\alpha + \rho^\beta$ computed with different theoretical methods for a given molecule usually are qualitatively similar, and often, the charge distributions also are quantitatively rather similar. In sharp contrast, the associated spin-density distributions $\rho^S = \rho^\alpha - \rho^\beta$ may vary widely and differ in major qualitative ways depending on the method used. The use of restricted open-shell theory (ROHF) for the computation of radicals completely suppresses spin polarization. However, unrestricted theory (UHF) allows for spin polarization, but its implementation also allows for an overestimation of spin polarization because UHF wave functions are not required to be eigenfunctions of the S^2 operator. This overestimation of spin polarization at the UHF level is called spin contamination. DFT methods also use UHF wave functions, but constraints are applied that limit the degree of spin contamination.[30]

Spin polarization intrinsically is an electron correlation effect, and the quality and reliability of spin-density distributions increases with the quality of the correlation treatment. Perturbation theory improves spin-density distributions, but second-order theory alone does not generally result in reliable spin densities. Effective spin-projection methods have been devised to remove spin contamination from UHF and from UMPx-level densities,[30,31] and we explored PUMPx levels up to fourth-order. For the systems studied here, the only way to ensure that the spin densities are reliable requires the computation of highly correlated wave functions with variational correlation methods, and we employ the QCISD level as our standard.

UHF Instability and Singlet Diradical Character. It is conceptually easy to understand how the presence of an unpaired electron may cause spin polarization. It is another matter to realize that spin polarization also might occur in

dx.doi.org/10.1021/tx2005458 | Chem. Res. Toxicol. 2012, 25, 620–633

Table 1. Relative Isomer Stabilities and Activation Energies Computed at B3LYP/6-31G* and QCI/6-31G*//B3LYP/6-31G* Levels

	DFT				QCI//DFT	
parameter	ΔE	ΔH_0	ΔH_{298}	ΔG_{298}	$\Delta E'$	$\Delta G'$
EA (**1**)	21.18	23.18	22.29	23.81	13.36	15.99
EA (**1**)[a]	34.72	36.48	36.36	37.04	27.90	30.22
			Protonation			
E_{rel}, **3b** vs **3a**	0.78	0.53	0.59	0.44	1.57	1.23
E_{rel}, **3c** vs **3a**	1.78	1.31	1.44	1.16	2.99	2.37
E_{rel}, **4a** vs **4b**	0.36	0.34	0.30	0.40	1.01	1.05
E_{rel}, **4c** vs **4b**	0.76	0.60	0.61	0.61	1.58	1.43
E_{rel}, **4d** vs **4b**	−0.02	−0.03	−0.03	−0.03	0.07	0.06
E_{rel}, **4c** vs **4a**	0.40	0.25	0.31	0.20	0.57	0.37
E_{rel}, **4b** vs **3a**	−1.26	−1.62	−1.52	−1.64	1.40	1.02
E_{rel}, **4b** vs **3a**[a]	−1.49	−2.04	−1.87	−2.14	1.76	1.11
PA (**2**, **3a**)	341.35	332.83	333.43	326.30	346.44	331.39
PA (**2**, **4b**)	342.61	334.45	334.95	327.94	345.04	330.37
PA (**2**, **3a**)[a]	327.72	319.18	319.84	312.55	332.47	317.30
PA (**2**, **4b**)[a]	329.21	321.23	321.72	314.69	330.71	316.19
			OH Loss			
E_{rel}, **6** vs **5**	13.07	12.58	12.58	12.68	12.42	12.03
$E_{rxn,}$ **2·3a** → **5** + **1** + H_2O	−62.1	−64.21	−63.96	−73.3	−60.3	−71.5
E_{rxn}, **3a** → **5** + OH	5.53	1.87	2.30	−7.74	0.52	−12.75
E_{rxn}, **4b** → **6** + OH	19.86	16.08	16.40	6.58	11.54	−1.74
E_{act}, **TS1** vs **3a**	6.45	4.99	4.86	5.01	13.05	11.61
E_{act}, **TS2** vs **4b**	14.88	12.88	12.96	12.63	20.75	18.50

[a]Use 6-31+G*.

Table 2. Relative Isomer Stabilities and Activation Energies Computed at the MP2(full)/6-31G* and QCI/6-31G*//MP2(full)/6-31G* Levels

	MP2				QCI//MP2	
parameter	ΔE	ΔH_0	ΔH_{298}	ΔG_{298}	$\Delta E'$	$\Delta G'$
EA (**1**)	−16.84	−18.58	−18.26	−18.28	8.73	7.29
EA (**1**)[a]	−1.02	−2.50	−2.32	−2.20	23.22	22.04
			Protonation			
E_{rel}, **3b** vs **3a**	1.73	1.23	1.32	1.09	1.42	0.78
E_{rel}, **3c** vs **3a**	3.14	2.28	2.47	2.05	3.04	1.95
E_{rel}, **4a** vs **4b**	0.54	0.50	0.45	0.56	0.92	0.94
E_{rel}, **4c** vs **4b**	1.00	0.63	0.74	0.53	1.63	1.16
E_{rel}, **4d** vs **4b**	0.13	0.11	0.12	0.11	0.17	0.15
E_{rel}, **4c** vs **4a**	0.46	0.13	0.28	−0.03	0.70	0.21
E_{rel}, **4b** vs **3a**	3.31	3.21	3.36	3.05	0.78	0.52
E_{rel}, **4b** vs **3a**[a]	4.13	3.83	4.04	3.62	1.08	0.57
PA (**2**, **3a**)	342.30	333.63	334.33	326.86	349.96	334.52
PA (**2**, **4b**)	338.99	330.42	330.97	323.82	349.18	334.01
PA (**2**, **3a**)[a]	326.85	318.30	319.02	311.57	335.92	320.64
PA (**2**, **4b**)[a]	322.72	314.47	314.98	307.95	334.84	320.07
			OH Loss			
E_{rel}, **6** vs **5**	13.64	13.05	13.05	13.12	14.05	13.53
E_{rxn} **2·3a** → **5** + **1** + H_2O	−121.47	−130.99	−129.59	−141.15	−63.67	−83.35
E_{rxn}, **3a** → **5** + OH	−22.70	−29.95	−28.99	−40.06	−1.72	−19.08
E_{rxn}, **4b** → **6** + OH	−12.37	−20.11	−19.29	−29.98	11.54	−6.07
E_{act}, **TS1** vs **3a**	36.08	33.75	33.77	33.59	14.16	11.67
E_{act}, **TS2** vs **4b**	39.94	36.09	36.54	35.24	20.15	15.45

[a]Use 6-31+G*.

molecules without overall spin. Ozone, O_3, is a well-known case of a molecule with singlet 1,3-diradical characteristics. Singlet ozone shows a UHF instability, that is, an unrestricted Hartree−Fock wave function results in a lower electronic energy as it allows α- and β-electrons to occupy different molecular orbitals. Ozone presents a case of a "triplet instability," even though the spin-polarized wave function describes a system without any net spin.[32,33] The term triplet instability is used to denote the number of unpaired electrons (a biradical) and not necessarily their net spin (singlet or

dx.doi.org/10.1021/tx2005458 | Chem. Res. Toxicol. 2012, 25, 620−633

Table 3. Mulliken Spin Populations Computed at the QCI//DFT Level

atom/group[a]	SP-1	2	3a	4b	SP-5	SP-6
O(N1), HO(N1)	0.294	0.238	0.458	0.006	0.128	-
N1	0.203	0.372	0.373	0.090	0.077	−0.274
N2	−0.226	0.085	−0.053	0.223	−0.136	0.142
C3	0.166	−0.030	0.073	−0.130	0.029	−0.153
$(C3)NH_n$	0.049	0.001	0.014	−0.024	0.020	−0.050
N4	−0.272	0.111	0.030	0.353	−0.080	0.230
O(N4), HO(N4)	−0.196	0.029	0.005	0.403	-	0.149
Σ_1	0.018	0.806	0.900	0.921	0.037	0.044
C4a	0.142	0.060	0.128	−0.110	0.017	−0.167
C5a	−0.150	−0.168	−0.158	0.078	−0.043	0.149
HC5	0.143	0.232	0.161	−0.047	0.078	−0.169
HC6	−0.140	−0.095	−0.097	0.101	−0.072	0.148
HC7	0.124	0.166	0.153	−0.045	0.048	−0.169
HC8, C8	−0.138	−0.001	−0.087	0.103	−0.065	0.164
Σ_2	−0.018	0.194	0.100	0.079	−0.037	−0.044
Σ_α	1.121	1.294	1.395	1.356	0.396	0.982
Σ_β	−1.121	−0.294	−0.395	−0.356	−0.396	−0.982

[a]See Scheme 1 for atom numbering.

Table 4. Mulliken Atom and Fragment Charges Computed at the QCI//DFT Level

atom/group[a]	1	SP-1	2	3a	4b	5	SP-5	6	SP-6
O(N1), HO(N1)	−0.431	−0.426	−0.562	−0.416	−0.055	−0.414	−0.422		
N1	0.068	0.048	−0.012	−0.029	−0.214	0.090	0.111	−0.270	−0.285
N2	−0.307	−0.302	−0.394	−0.324	−0.317	−0.300	−0.317	−0.319	−0.312
C3	0.740	0.732	0.671	0.701	0.712	0.650	0.664	0.720	0.712
$(C3)NH_n$	−0.031	−0.031	−0.129	−0.062	−0.058	−0.062	−0.056	−0.037	−0.034
N4	−0.228	−0.208	−0.268	−0.391	−0.236	−0.550	−0.567	−0.198	−0.170
O(N4), HO(N4)	−0.546	−0.544	−0.668	−0.066	−0.460	-	-	−0.518	−0.535
Θ_1	−0.734	−0.730	−1.361	−0.587	−0.627	−0.586	−0.586	−0.622	−0.624
C4a	0.314	0.299	0.296	0.265	0.276	0.238	0.246	0.317	0.303
C5a	0.235	0.246	0.262	0.284	0.281	0.238	0.229	0.158	0.167
HC5	0.074	0.065	−0.033	0.038	0.005	0.069	0.070	0.055	0.051
HC6	0.015	0.022	−0.060	0.008	0.017	−0.001	−0.001	0.008	0.015
HC7	0.039	0.032	−0.057	0.007	0.002	0.031	0.033	0.029	0.025
HC8, C8	0.058	0.065	−0.046	−0.016	0.046	0.010	0.009	0.054	0.063
$\Theta_2 = -\Theta_1 + n$	0.734	0.730	0.361	0.587	0.627	0.586	0.586	0.622	0.624
Θ_+	1.543	1.511	1.229	1.304	1.339	1.327	1.363	1.342	1.336
$\Theta_- = -\Theta_+ + n$	−1.543	−1.511	−2.229	−1.304	−1.339	−1.327	−1.363	−1.342	−1.336

[a]See Scheme 1 for atom numbering. Charge of system, *n*.

triplet). Similar UHF instabilities have recently been reported for conjugated macrocycles,[34] for fullerenes and nanotubes,[35] and for nitro compounds and related species.[36]

The B3LYP wave functions of **1**, **5**, and **6** do not show UB3LYP instabilities. We used various methods to generate spin-polarized UB3LYP guess wave functions, and all of these returned to the respective spin-free RB3LYP wave function. However, we found that spin-polarized UHF singlet wave functions of **1**, **5**, and **6** are more stable than the respective RHF wave functions, and UQCISD computations using the spin-polarized UHF wave functions resulted in spin-polarized UQCISD electron densities. For each system, we expected the UQCI energy to be *lower* than the respective RQCI energy, that is, we expected the molecule to prefer the spin-polarized singlet wave function and that the spin-free singlet was merely an artifact of using restricted wave function. However, the energies of the spin-polarized UQCISD solutions are *higher* than the respective RQCISD energies for **1**, **5**, and **6**. The lower RQCISD energies of **1**, **5**, and **6** are listed in Table S2 (Supporting Information), and the UQCISD energies are given in footnote c to Table S2 (Supporting Information). The spin-polarized solutions are 7−8 kcal/mol above the spin-free densities (footnote d, Table S2 (Supporting Information)). This outcome means that molecules **1**, **5**, and **6** can exist in two singlet states, the spin-free singlet ground state and the spin-polarized singlet excited state. This outcome also means that the UHF instabilities in these cases actually are artifacts at the Hartree−Fock level (artificially favoring the spin-polarized singlet). The artificial UHF instability helped to discover the spin-polarized UQCISD densities, and the latter are real nevertheless. In the absence of the UHF instability, one simply would generate a spin-polarized reference wave function in some other way, and we did just that to compute the spin-polarized UQCISD densities for the DFT-optimized structures.

Population Analysis: Spin Polarization versus Spin Uncoupling. In Table 3 are listed the Mulliken spin populations computed at the UQCI//DFT level, and these data are discussed. The respective UQCI//MP2 level data are

dx.doi.org/10.1021/tx2005458 | Chem. Res. Toxicol. 2012, 25, 620−633

Scheme 2. Electronic Structures of Ozone, Diazene Oxide, and Imine Oxide

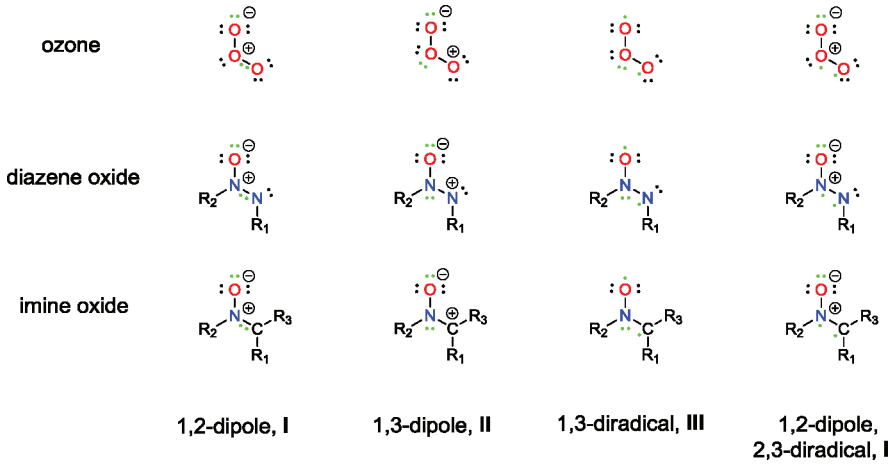

provided in Table S3 in Supporting Information. Spin populations for hydrogen atoms are included with the spin population of the atom to which the H atoms are attached. To assess the extent of spin delocalization into the benzene ring, we define the parameters Σ_1 and Σ_2. The values Σ_1 and Σ_2 provide the overall spin populations of the heterocyclic arc (N1−N2−C3−N4 with exocyclic attachments) and of the benzene ring (C4a−C5a−C5−C6−C7−C8 with attached H-atoms), respectively. To assess the overall extent of spin polarization, we define and report the parameters Σ_α and Σ_β. The values Σ_α and Σ_β are the sums of the spin populations of all fragments with net α- or β-spin populations, respectively. These parameters have been absolutely essential to develop some understanding of the radical species and to characterize some of the extraordinary spin cases encountered.

A singlet system with $0 < \Sigma_\alpha < 0.2$ and $-0.2 < \Sigma_\beta < 0$ describes essentially a closed-shell molecule with "some biradical character." In contrast, a singlet system with $\Sigma_\alpha \approx 1$ and $\Sigma_\beta \approx -1$ essentially contains two unpaired electrons of opposite spin. Doublet radicals that feature $1 < \Sigma_\alpha < 1.2$ and $-0.2 < \Sigma_\beta < 0$ describe a "normal" system with one unpaired electron and some spin polarization, while doublet radicals with $1 < \Sigma_\alpha < 1.4$ and $-0.4 < \Sigma_\beta < 0$ are heavily spin-polarized. On occasion, one encounters doublet radicals with $\Sigma_\alpha \approx 2$ and $\Sigma_\beta \approx -1$, and systems of this type exhibit so-called "quartet instabilities" and contain essentially three unpaired electrons. As with the term triplet instability, the term "quartet instability" denotes the number of unpaired electrons (a triradical rather than a monoradical) and not necessarily the net spin (doublet or quartet).

Mulliken charges computed at the UQCI//DFT level are listed in Table 4, and these data are discussed; the respective UQCI//MP2 level data are provided in Table S4 (Supporting Information). To assess the extent of charge distribution within the two ring systems, we define the parameters Θ_1 and Θ_2, respectively, in analogy to Σ_1 and Σ_2, respectively. To quantify the notion of "internal polarization," we define and the parameter Θ_+ as the sums the charges of all fragments with net (+)-charge. In analogy, the parameter Θ_- equals the sums the charges of all fragments with net (−)-charge and $\Theta_- = -\Theta_+ - n$, where n is the overall charge of the system.

Spin-Density Distributions. The analysis of the spin-density distributions provides direct information as to the relative importance of the various resonance forms, and QCI spin-density distributions will be shown for two values of ρ^S and based on the DFT structures (vide infra, cf. Figure 2). The surface computed with the higher setting of $\rho^S = 0.002$ e au^{-3} allows for the identification of the major radical sides and the recognition of the major mechanism of spin delocalization. However, the lower setting of $\rho^S = 0.0004$ e au^{-3} reveals details of spin polarization. Note that we discuss only QCI spin densities throughout this article. We also computed the spin-density distributions at the DFT and MP2 levels, and they are provided as Supporting Information.

Structures of 1 and 2 and Electron Affinities of 1. 1,2,4-Benzotriazine is a perfectly fine 10-electron heteroarene, and its π-system apparently remains intact upon 1,4-*N*,*N*-dioxide formation. As with aniline,[37] the lone pair of the NH_2-group in **1** (BTO, 1,2,4-benzotriazine 1,4-*N*,*N*-dioxide) remains localized on the pyramidal amino-*N* atom. The 3-amino group engages in intramolecular H-bonding with O(N4) (d(O···H): DFT: 2.14 Å; MP2: 2.16 Å) in **1**, and the angles at C3 support the argument that the nitrogen lone pair is not localized into the benzotriazine ring in that the NH_2 group as a whole is bent to strengthen the H-bond (DFT: $\angle$(N4−C3−NH_2) = 115.2°; $\angle$(N2−C3−NH_2) = 119.7°; MP2: $\angle$(N4−C3−NH_2) = 114.9°, $\angle$(N2−C3−NH_2) = 120.0°).

One-electron reduction of **1** to **2** destroys the aromatic system, and the DFT and MP2 optimized structures of **2** are drastically different. The DFT structure of **2** retains the essentially planar heteroarene, whereas the MP2 structure of **2** contains a concave triazine with both N1 and N4 adopting markedly pyramidal geometries. The DFT and MP2 structures both feature *more* pyramidal NH_2 groups and *shorter* H-bonds (DFT, 2.02 Å; MP2, 1.96 Å) from the NH_2 hydrogens to the neighboring oxygen. The computed electron affinities of **1** (negative value of the reaction energy of **1** + e^- → **2**) are reported in Tables 1 and 2, the values show large qualitative theoretical model dependencies, the computed ΔE values are 21.2 (DFT), 13.4 (QCI//DFT), −16.8 (MP2), and 8.7 kcal/mol (QCI//MP2), and, quite obviously, there is a problem with the *negative* value computed at the MP2 level.

Considering that **2** is an anion, part of the theoretical level dependency clearly is caused by the lack of diffuse functions in the 6-31G* basis set. Thus, we computed **1** and **2** again with diffuse functions added to the basis set, that is, at the B3LYP/6-31+G* and MP2(full)/6-31+G* levels. The additional diffuse functions do not affect the structures of **1** and **2** drastically, and

dx.doi.org/10.1021/tx2005458 | *Chem. Res. Toxicol.* 2012, 25, 620−633

Scheme 3. Electronic Structures of Neutral 1,4-*N*,*N*-Dioxide 1 and of Radical Anion 2

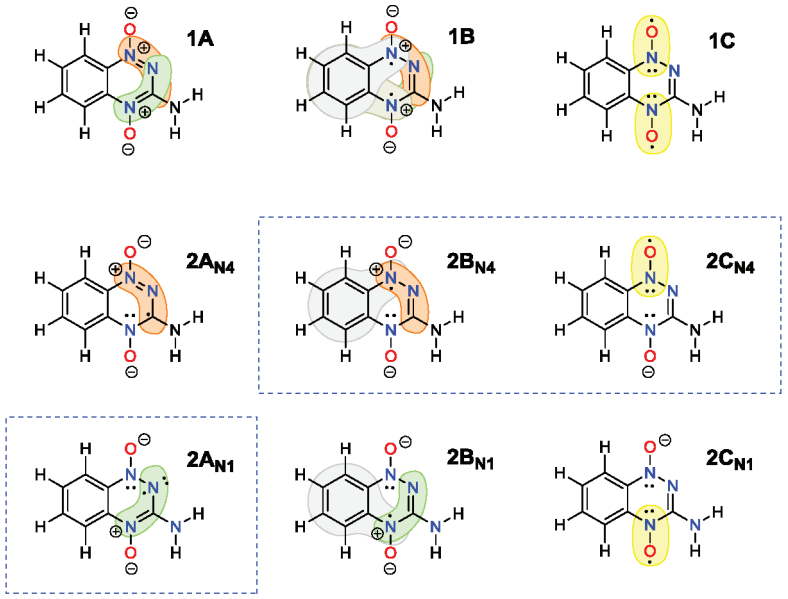

as expected, the energies of anion **2** are lowered much more compared to **1**. The electron affinities computed with the 6-31+G* basis set all increase, and the ΔE values now are 34.7 (DFT), 27.9 (QCI//DFT), −1.0 (MP2), and 23.2 kcal/mol (QCI//MP2). Note that the MP2-derived electron affinity is still negative. Hence, the theoretical level dependency indicates a deeper difference between the DFT and MP2 methods. The QCI computations correct deficiencies of the reference wave functions and suggest that the DFT results are more realistic because the QCI//DFT and QCI//MP2 data are in qualitative agreement, and the data show especially large changes between MP2 and QCI//MP2 data. In the following section, we address the question, what are the origins of this large theoretical level dependency, and how is one to think of the electronic structures of substrate **1** and anion **2**?

Electronic Structures of *N*,*N*-Dioxide 1 and Radical Anion 2. We begin by pointing out the analogy between the electronic structures of ozone, diazene oxide, and imine oxide (Scheme 2). None of these molecules can be described adequately by just one Lewis structure, and instead, one must discuss a variety of resonance forms for each molecule and determine which resonance forms are important and which ones are only minor contributors to this molecule's electronic structure. In each case, the familiar resonance forms **I** (1,2-dipole), **II** (1,3-dipole), and **III** (1,3-diradical) are shown of the 3-center-4-electron π-system (π-electrons indicated in green for clarity) along with the less familiar form **IV** (1,2-dipole and 2,3-diradical). Resonance form **1A** (Scheme 3) represents a 6-center-8-electron π-system extending over the arc (O−N1−N2−C3−N4−O) of **1** which joins the 1,2-dipole diazene oxide with the 1,2-dipole imine oxide via their respective R_1 positions. The joining of two 1,3-dipoles **II** is disadvantaged because it would place like charges next to each other and was not considered. Resonance forms **1B** and **1C** are related to **IV** and **III**, respectively.

The spin-free singlet ground state is best described by **1A** (with small contributions by **1B** and **1C**) and this is consistent with the near-planar structure of **1**. The spin-polarized singlet excited state density is best described by **1B** ↔ **1C** (with a small contribution from **1A**). Structure **1C** shows electron density accumulation at N1 and N4, and there is the potential for pyramidalization in the optimized structure of the spin-polarized singlet excited state. The UQCISD//DFT spin-density distribution of **SP-1** (Figure 2) shows a heavily spin-polarized diradical with $\Sigma_\alpha \approx 1.1$ and $\Sigma_\beta \approx -1.1$ (Table 3) with nearly equal spin populations in the (N1,O) and (N4,O) regions (about $|\rho^S| = 0.5$). Spin delocalization away from the NO regions into the phenyl ring (shaded gray in Scheme 3; RFs not shown) and over the two diazaallyl systems (orange and green shading; RFs not shown) occurs over the entire framework of **SP-1** and reflects the mutual enhancement of the spin delocalization and spin polarization caused by the (N1,O) and (N4,O) regions.

Starting with the diradical resonance forms **1B** and **1C** (Scheme 3), one can consider the consequences of adding an electron either to N1 or N4, respectively, to generate **2B$_{N1}$** and **2B$_{N4}$**, respectively, or to one of the attached O atoms to generate **2C$_{N1}$** and **2C$_{N4}$**, respectively. As with **SP-1**, the N-centered radical may delocalize over the phenyl ring (gray shading; RFs not shown) and/or over one diazaallyl system, either the 1,2-diazaallyl (**2A$_{N4}$**, orange shading) or the 1,3-diazaallyl system (**2A$_{N1}$**, green shading).

The UQCI//MP2 and UQCI//DFT spin-density distributions (Figure 2) show that radical anion **2** is a doublet system with one unpaired electron and significant spin polarization ($\Sigma_\alpha = 1.3$, $\Sigma_\beta = -0.3$). The data also very clearly show more spin density in the (N1,O) region than in the (N4,O) region in agreement with the results of EPR studies (vide supra). The overall spin population of the (N1,O) fragment is about 0.61, and the spin populations suggest a slightly higher importance for **2B$_{N4}$** (N1-radical) than for **2C$_{N4}$** (O(N1)-radical). The overall spin population of the (N4,O) fragment is only about 0.14, and **2B$_{N1}$** (N4-radical) and **2C$_{N1}$** (O(N4)-radical) are much less important. Roughly speaking, a spin population of about 0.3 has been delocalized out of the NO regions and placed on N2 (ρ^S(N2) = 0.09) and in the benzene ring (Σ_2 = 0.19). This spin-distribution pattern fits with delocalization over the 1,3-diazaallyl system (**2A$_{N1}$**, green shading).

Nonplanar Structures of Neutral Radicals 3 and 4. The analysis of the electronic structure of **2** (Scheme 3) is expanded

dx.doi.org/10.1021/tx2005458 | *Chem. Res. Toxicol.* 2012, 25, 620−633

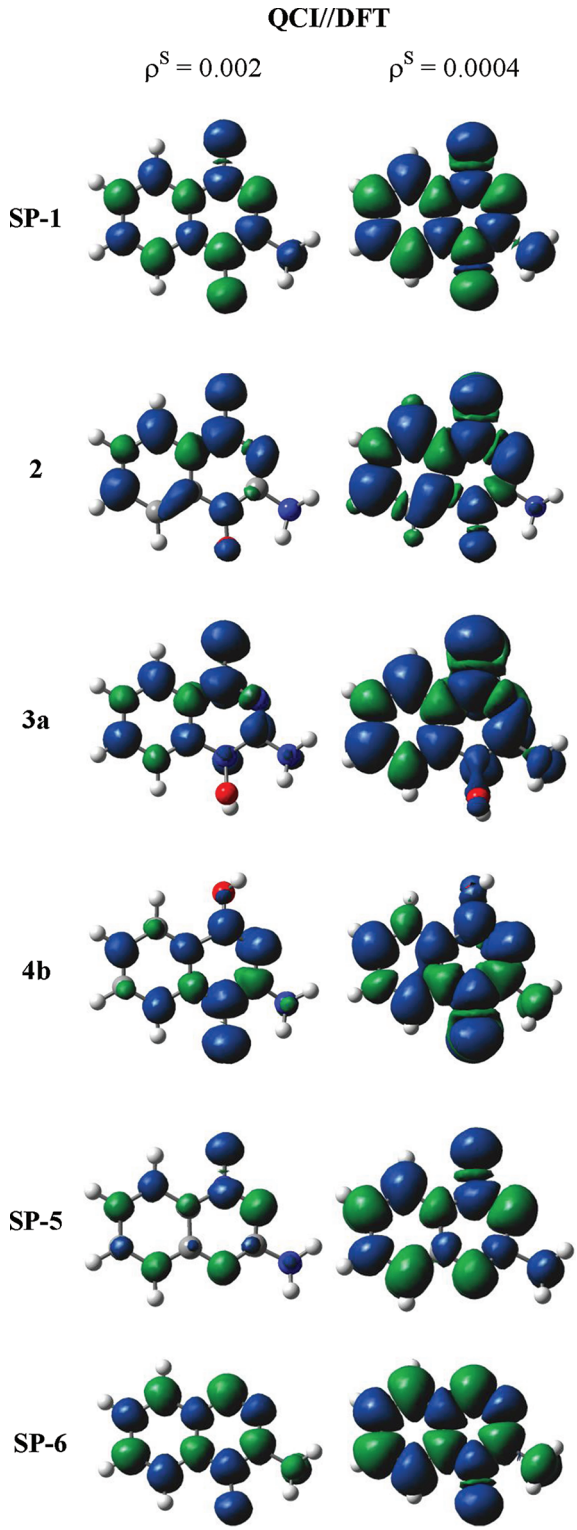

Figure 2. Spin-density distributions computed at the UQCISD level based on the DFT structures for radicals **2**–**4** and for spin-polarized singlet excited states of **1**, **5**, and **6**. An expanded version of this figure also contains the QCI//MP2 spin-density distributions, and it is in Supporting Information.

to the neutral radicals **3** and **4** (Scheme 4) formed by protonation of **2** at O(N4) or O(N1), respectively. As with **2**, we note that the amino-group is pyramidal and therefore consider only resonance forms that retain a neutral NH_2 group. Protonation of **2** removes one of the resonance forms $\mathbf{2C_{N1}}$ and $\mathbf{2C_{N4}}$: only $\mathbf{3C_{N4}}$ exists for isomer **3** and only $\mathbf{4C_{N1}}$ for isomer **4**. Without $\mathbf{3C_{N1}}$, the importance of $\mathbf{3B_{N1}}$ also is diminished because of the loss of $\mathbf{3B_{N1}} \leftrightarrow \mathbf{3C_{N1}}$, and without $\mathbf{4C_{N4}}$, the importance of $\mathbf{4B_{N4}}$ is diminished for the analogous reason. The quasi-degeneracy of the NO regions in **1** is diminished to near-degeneracy by reduction to **2**, and it is effectively removed by protonation to isomers **3** and **4**.

The spin density becomes more localized in **3** and **4** compared to **2**, in the (N1,O) region in **3** (ρ^S(N1,O) = 0.83 ≫ ρ^S(N4,OH) = 0.04) and in the (N4,O) region in **4** (ρ^S(N1,OH) = 0.10 ≪ ρ^S(N4,O) = 0.76). The spin-density localization in the (N1,O) region in **3** enhances the spin-density distribution of **2**, whereas the formation of **4** localizes spin density in the (N4,O) region and requires major spin-density relaxation compared to **2**.

The high spin density in the (N1,O) region of **3** and the negligible spin density at C3 of **3** (ρ^S(C3) = 0.07; ρ^S(C3–NH_2) = 0.09) provide clear and strong evidence that the LDRMP radical is the dominant resonance form and that the C3-centered LWR radical is merely a minor contributor.

Planarity of the heteroarene requires that both N1 and N4 are part of diazaallyl systems. As soon as one of the diazaallyl stabilization mechanisms (i.e., allyl-type delocalization of N1 spin density onto C3 or of N4 spin density onto N2) dominates, either N1 or N4 will feature lone pair localization and a tendency to pyramidalize. The 1,2-diazaallyl resonance forms $\mathbf{3A_{N4}}$ and $\mathbf{3B_{N4}}$ and the O-radical form $\mathbf{3C_{N4}}$ feature a lone pair at N4, the N atom with the OH group, and this lone pair manifests itself in the structure of **3**, which is clearly pyramidal at N4. The structure of **4** shows pyramidalization of N1, the N atom that carries the OH group, consistent with $\mathbf{4A_{N1}}$, $\mathbf{4B_{N1}}$, and $\mathbf{4C_{N1}}$.

Stereoisomers of 3 and 4 and Molecular Flexibility. With N4(**3**) and N1(**4**) pyramidal and with a pyramidal NH_2 group present, one may expect four stereoisomers for **3** and **4**. The number of possible stereoisomers doubles in light of the fact that the hydroxyl-H may point to the concave or the convex faces of nonplanar **3** or **4**.

Side views of stereoisomers of **3** are shown in the first two rows of Figure 3: all are chiral, and we show the enantiomers with the same chirality at N4. The OH bond points to the convex and concave faces in **3a** and **3b**, respectively. The search for isomers of **3a** and **3b** with inverted NH_2 groups lead to **3c**, the amino-*N* inverted version of **3b**, while a stationary structure of type **3d** could not be located. Intramolecular H-bonding is possible in **3a**–**3c** but would not be possible in **3d**. The order of stability is the same at all levels, **3a** > **3b** > **3c**. At the DFT level, the relative ΔG_{298} values are 0.4 and 1.2 kcal/mol for **3b** and **3c**, respectively, and at the MP2 level, the values are 1.1 and 2.1 kcal/mol, respectively. The relative $\Delta G'$ values computed at the QCI//DFT level are 1.2 and 2.4 kcal/mol for **3b** and **3c**, respectively, and at the QCI//MP2 level, the values are 0.8 and 2.0 kcal/mol, respectively.

In the bottom rows of Figure 3 are shown side views of the respective enantiomers of stereoisomers of **4**. The direct through-space interaction between the OH and NH_2 groups is not possible in **4**, and all four minima exist. The OH bond points to the convex face in **4b** and **4d**, while it points to the concave face in **4a** and **4c**. Minima **4a** and **4c** and structures **4b** and **4d** are pairwise epimers due to NH_2 group inversion. The order of stability is the same at all levels with **4b** ≈ **4d** > **4a** ≈ **4c**. There are tiny differences in the stabilities of **4b** and **4d** and of **4c** and **4a**, but there is a clear and noticeable preference of

dx.doi.org/10.1021/tx2005458 | *Chem. Res. Toxicol.* 2012, 25, 620–633

Scheme 4. Electronic Structure of Radicals 3 and 4

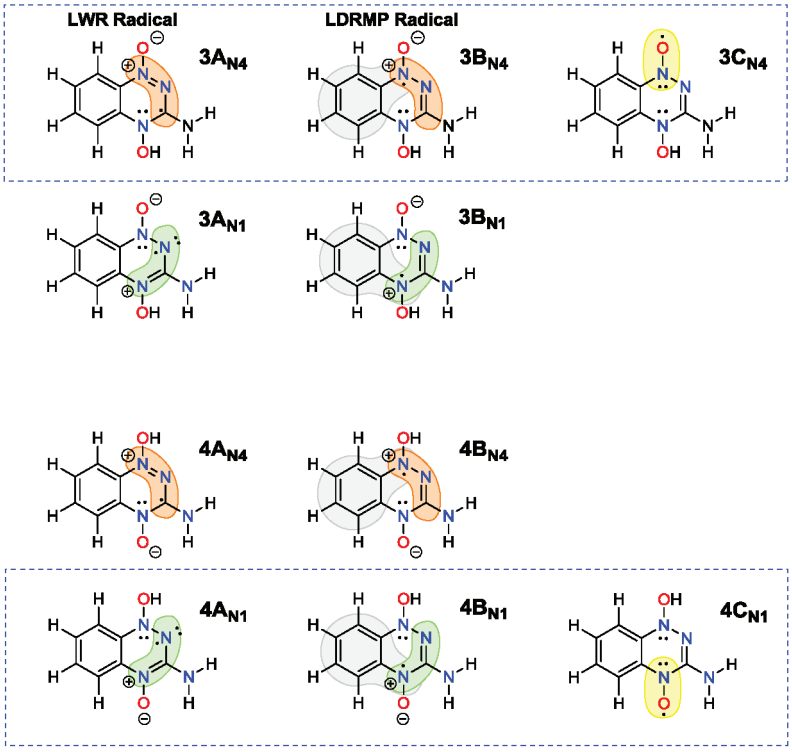

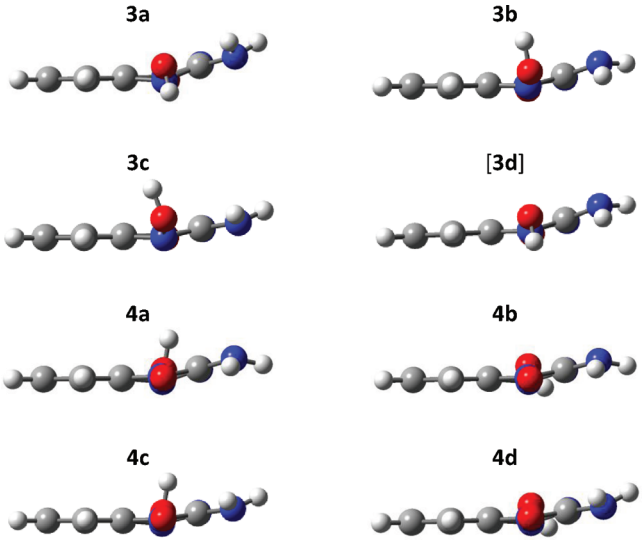

Figure 3. Side views of stereoisomers of **3** and **4**. The B3LYP/6-31G* structures are shown.

$\Delta G_{298} \approx 0.5$ kcal/mol for the former pair over the latter at the DFT and MP2 levels, and the $\Delta G'$ values ≈1−1.4 kcal/mol are slightly higher.

Isomer Preference Energy of 3 and 4 and Proton Affinities of 2. The relative energies of **3** and **4** and the proton affinities of **2** (negative value of the reaction energy of **2** + H^+ → **3**/**4**) were determined with the 6-31G* and 6-31+G* basis sets (Tables 1 and 2). There is a small preference for **3a** over **4b** at the QCI level, and irrespective of the basis set and/or the level of structure optimization, $\Delta G'$(QCI//DFT) = 1.1 and $\Delta G'$(QCI//MP2) = 0.6 kcal/mol. The respective values computed at the levels of optimization are ΔG(DFT) = −2.1 kcal/mol and ΔG(MP2) ≈ +3.6 kcal/mol. The $\Delta G'$(QCI//MP2) and ΔG(MP2) have the same sign, while the DFT based values do not. This observation should not be seen as an endorsement of the perturbation method, and instead, the numbers again demonstrate that higher level correlation methods are required to obtain consistently meaningful results.

There exists some confusion about the relative stabilities of **3** and **4** for various reasons. To begin with, Li et al.[18] reported $\Delta H_0 = -1.3$ kcal/mol (i.e., a preference for **4** over **3**) at the B3LYP/6-31G*, level while our value at the same level is $\Delta H_0 = -1.6$ kcal/mol. This minor difference is due to the fact that Li et al. compared **3a** to **4a**, while we compare **3a** to the more stable structure **4b**. Li et al. also found a very similar preference of $\Delta H_0 = -1.1$ kcal/mol for **4** at the B3LYP/6-311+G* level but a preference of $\Delta H_0 = +6.2$ kcal/mol for **3** over **4** when aqueous solvation was considered at the PCM(B3LYP/6-311+G*) level. Hence, the results by Li et al. would suggest that the preference for **3** is not intrinsic but that it is the consequence of solvation. Our QCI results show that the first statement does not hold. While solvation does not cause the preference for **3**, solvation may still enhance this preference, but IEF-PCM (integral equation formalism PCM[38]) solvation studies suggested only modest effects on the TPZ species.[17]

The proton affinities of **2** to form **3** or **4** are about $\Delta G' = 319 \pm 2$ kcal/mol at the QCI/6-31+G* levels (Tables 1 and 2), and the magnitude is remarkable. The gas phase proton affinities of HO^- and RO^- fall in the range 375−390 kcal/mol,[39] those of carboxylates are 345−350 kcal/mol,[40] and the proton affinity of peroxynitrite is 347.1 kcal/mol,[41] and all of these are significantly higher than PA(**2**). In fact, PA(**2**) compares to the proton affinities of Cl^- (333 kcal/mol) and Br^- (323 kcal/mol).[38] Laderoute determined pK_a(**3**)[42] = 6 in aqueous solution based on the rate k_{obs} for the disproportionation 2 **3** → **5** + **1** + H_2O and assuming two bimolecular paths for disproportionation (2 **3** → **5** + **1** + H_2O; **3** + **2** + H^+ → **5** + **1** +

dx.doi.org/10.1021/tx2005458 | Chem. Res. Toxicol. 2012, 25, 620−633

Scheme 5. Electronic Structure of 5 and 6

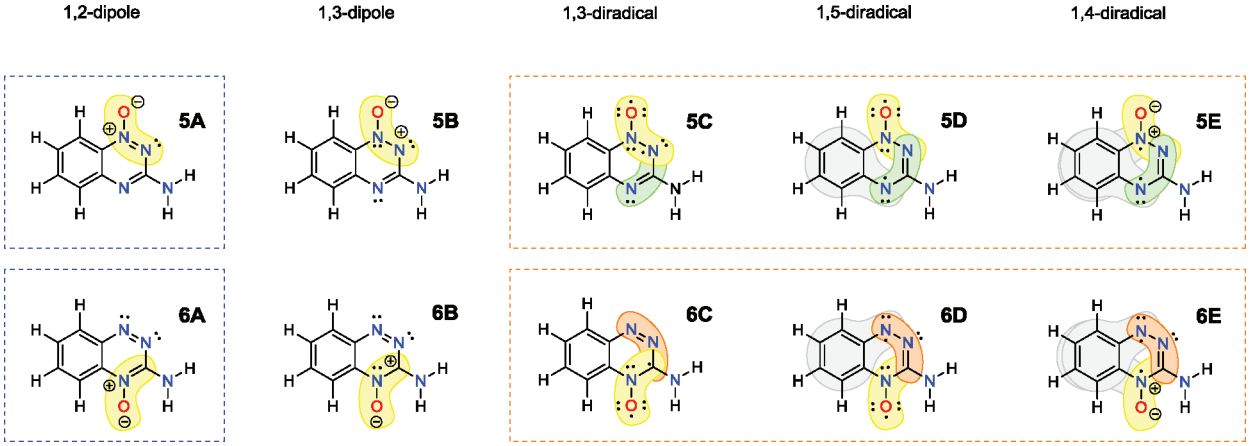

H_2O). The consideration of N−OH dissociation as an *additional* reaction channel for the reaction **3** → **5** (vide infra) would suggest that pK_a(**3**) actually is *lower* than 6. Irrespective of whether pK_a(**3**) is 6 or lower, it is clear that the ratio [**2**]/[**3**] ≫ 1 in neutral and basic solution ([**2**]/[**3**] ≥ 10 at pH = 7, [**2**]/[**3**] ≥ 10^4 at pH = 10).

N−OH Homolysis and Isomeric 3-Amino-1,2,4-benzotriazine Monoxides. Homolysis of the N−OH bond of **3** or **4** generates ·OH and neutral 3-amino-1,2,4-benzotriazine monoxide **5** or **6**, respectively. The structures of **5** and **6** and the reaction transition state structures **TS1** and **TS2** are shown in Figure 1. The bond length *d*(N−O) of the bond that is being broken is significantly longer in **TS1** compared to **TS2** irrespective of the level of optimization: **TS1**, *d*(N1−O) = 1.926 (DFT), 1.916 (MP2); **TS2**, *d*(N4−O) = 1.713 (DFT), 1.775 (MP2). This is noteworthy because the more exothermic reaction apparently has the later transition state. We believe that this feature is caused by the stabilization of the OH group in **TS1** by way of hydrogen-bonding with the amino-group: **3a**, *d*(O···H(NH_2)) = 2.240 (DFT), 2.228 (MP2); **TS1**, *d*(O···H-(NH_2)) = 2.259 (DFT), 2.282 (MP2).

A rather strong preference is found for monoxide **5** over **6**, and the Δ*G* and Δ*G*′ values computed with the DFT and MP2 structures all fall within the narrow range of 12−13.5 kcal/mol (Tables 1 and 2). Considering the possibly attractive neighboring interaction between the amino group and the negatively charged oxygen, one might have expected a preference for **6**.

Molecules **5** and **6** can exist in two singlet states, the spin-free singlet ground state and the spin-polarized singlet excited state (vide supra), which is about 8 ± 1 kcal/mol higher in both cases. Using the resonance forms shown in Scheme 5, the spin-free singlet ground state is best described by **5A** (with small contributions by **5B**−**5E**), and the spin-polarized singlet excited state density is best described by **5C** ↔ **5D** ↔ **5E** (with small contributions from **5A** and **5B**). Form **5C** is the 1,3-diradical of the diazene oxide moiety, **5D** accounts for the presence of the 1,3-diazaallyl, and 1,4-diradical **5E** can be seen as the diazaallyl variety of the 1,2-dipole, 2,3-diradical (**IV** in Scheme 2). The spin-free singlet ground state and the spin-polarized singlet excited state of **6** can be described in analogy with **6A**−**6E**.

The spin populations show a significant difference between the spin-polarized electronic structures **SP-5** and **SP-6**, respectively, in that Σ_α(**SP-5**) = 0.40, whereas Σ_α(**SP-6**) = 0.98 (Table 3). The electronic structure of **SP-6** really is that of a diradical: a full α- and a full β-spin are present and distributed over the molecule. However, the electronic structure of **SP-5** presents an interesting case of "incomplete unpairing," and we refer to such a case as singlet diradicaloid. One may expect that the diradicaloid nature of **SP-5** can be tuned by suitable substituents. It will be interesting to explore this possibility in cases where the diradicaloid species is thermodynamically preferred. Even if the ground state remains closed-shell, the easy accessibility of this biradical state may be relevant to the ability of these molecules to react with carbon-centered radicals in a manner that ultimately leads to oxygen transfer to the organic radical.[43] In light of the diradical character of **SP-6**, it is particularly noteworthy that it is compound **6** that showed the highest rate of reaction with a carbon-centered DNA radical among **1**, **5**, and **6**.[42a]

C3 Electron Hole and C3−N2 Bond Polarity. TPZ carries an amino group at C3 (X = NH_2), and a variety of analogues have been studied in which this amino group was replaced by other groups (X = H, CH_3, Ph, OMe, ...).[44,45] This replacement is usually motivated by consideration of the LWR-radical structure of intermediate **3** and the notion that X might help stabilize the spin density at C3. For isomer **4**, one also can write a resonance form with the radical at C3. Our results show, however, that **3** and **4** are not C3-centered radicals, and instead, our analysis shows high spin densities in the (N1,O)-region of **3** and in the (N4,O)-region of **4**. In the case of **3**, the spin-density analysis supports and corroborates the LDRMP-radical notation originally suggested by Lloyd et al.[6]

Radical sites are locations of electron deficiency, and they are best placed in regions that can compensate through high electronegativity. The population data of Table 4 help to make this point. Electron density accumulation occurs on the electronegative atoms of the triazene, and the Θ_1 values all are very negative, Θ_1 = −0.7 ± 0.2. Contained in this rather electron-rich triazene, C3 is extraordinarily deprived of electron density in all of the systems listed in Table 4 with charges of *q*(C3) = +0.7 ± 0.2. For C3 to be part of the very electron-rich region turns out to be a really bad thing: C3 is deprived of electron density by the attached heteroatoms, and C3 does not get any benefit from the huge overall electron-excess in the triazene.

There is no doubt that the variation of the C3-substituent X affects the outcome of the reduction/protonation sequence **1** → **2** → **3** and/or **4** in significant ways. If X does not affect this chemistry through its radical-stabilizing ability, then X must

dx.doi.org/10.1021/tx2005458 | *Chem. Res. Toxicol.* 2012, 25, 620−633

affect the electron density at C3 and the molecular polarity. The population analysis shows that the N2−C3(X) moiety is highly polar, and hence, the dipole moment of the C3−N2 bond is very large. Considering that the bond dipole moments of the NO moieties have their (+) pole on N, there naturally exists an incentive to increase the N1−O bond polarity and to reduce the N4−O bond polarity, and the strength of this incentive depends on X. This issue contributes to the preference for protonation at O(N4).

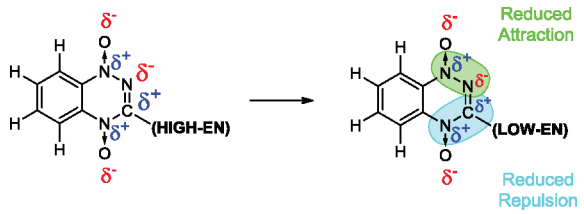

The data in Table 4 show that the charge distributions in the closed-shell systems **1**, **5** and **6** are rather similar to those in the respective spin-polarized electronic states **SP-1**, **SP-5** and **SP-6**. Hence, a large change in the spin density distribution can be achieved without major reorganization of the total electron density distribution.

Reaction Energies and Activation Barrier for N−OH Homolysis. The N−OH homolysis of **3** is almost thermoneutral (QCI//DFT, $\Delta E'$ = 0.5; QCI//MP2, $\Delta E'$ = −1.7 kcal/mol), whereas the N−OH homolysis of **4** is endothermic (QCI//DFT, $\Delta E'$ = 11.5; QCI//MP2, $\Delta E'$ = 11.5 kcal/mol). The dissociation reactions in the gas phase benefit very much from the entropy term, and the free enthalpies all are negative. The reaction free enthalpies computed for the N−OH homolysis of **3** are $\Delta G'$ = −12.8 (QCI//DFT) and −19.1 kcal/mol (QCI//MP2). The reaction energy profiles for the N−OH homolyses of **3** and **4** are drawn together and to scale in Figure 4 based on the $\Delta G'$ date computed at the QCI//DFT (blue) and QCI//MP2 (red) levels.

The QCI//DFT and QCI//MP2 activation barriers $\Delta G'$ ($\Delta E'$) for hydroxyl loss from **3** are 11.6 (13.1) and 11.7 (14.2) kcal/mol, respectively. By contrast, the activation barriers $\Delta G'$ ($\Delta E'$) for hydroxyl radical loss from **4** are 18.5 (20.8) and 15.5 (20.2) kcal/mol, respectively. The activation barriers computed at the QCI-level for the reaction via **TS1** are consistent with the experimental dissociation energy of ΔG_{exp} = 14 kcal/mol estimated in neutralization−reionization mass spectrometry experiments.[13]

The 1-oxide **5** is the major mono-N-oxide TPZ metabolite (90−95%) formed together with a small amount of 4-oxide **6** (5−10%).[10] This experimental outcome is consistent with the findings that OH loss from **3a** is preferred kinetically and thermodynamically compared to **4b**. The fact that **6** is formed in measurable yield reflects the relatively low activation barriers for the dissociations of **3a** and **4b** and suggests that the recombination **6** + HO· → **4b** is not effective.

The consideration of all structural possibilities is important, and the lack of a complete characterization of the potential energy surfaces can cause significant error. For example, Li et al.[18] computed activation barriers for the reactions **3** → **5** + ·OH and **4** → **6** + ·OH, respectively, at the B3LYP/6-31G* level and reported activation barriers ΔH_0 of 5.0 and 15.6 kcal/mol, respectively. While their value for the reaction of **3** agrees with our ΔH_0 value determined with **3a**, Li's ΔH_0 value for **4** is based on conformation **4a**, while our value ΔH_0 = 12.9 kcal/mol is based in **4b**. The same structural issue occurs with **TS2**; Li's value H_0(**TS2**) = −640.08561 au is significantly higher than our value H_0(**TS2**) = −640.09048 au.

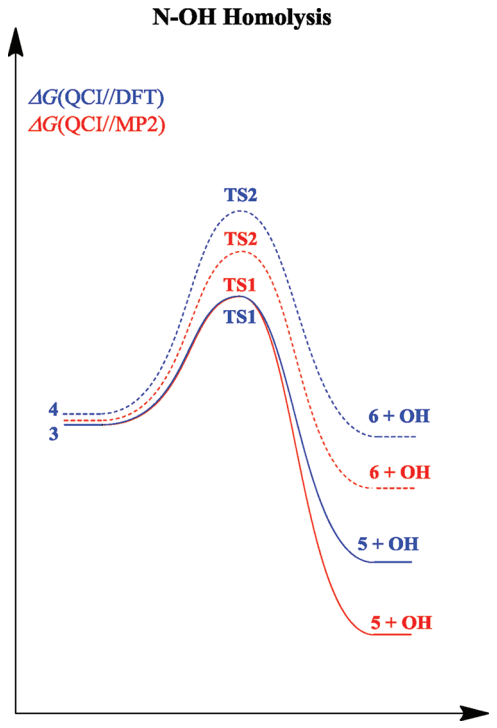

Figure 4. Free enthalpy surfaces for reactions of isomers **3** (solid) and **4** (dashed) as computed at the QCI//DFT (blue) and QCI//MP2 (red) levels.

Isotropic Hyperfine Coupling Constants. We computed isotropic hyperfine coupling constants a for ^{14}N (I = 1, 99.6%) and ^{1}H atoms in radicals **2** and **3** using their QCI//DFT spin-density distributions, and the results are summarized in Table 5. The hyperfine coupling constant a_A informs about the magnitude of the electron spin density in the proximity of the respective nuclear magnetic moment of atom A, ρ^S(A), and there is no general correlation between the overall spin population of an atom's basin and the spin density close to the atom's nucleus. Comparison of the a values computed for **2** and **3** shows significant similarities, and consequently, it would be extremely difficult to distinguish one from the other or to decide whether one of both of the radicals contribute to the EPR spectrum.

The product of reduction of **1** has been detected by EPR spectroscopy by Lloyd et al.[6] and by Anderson et al.,[17] and their a values are included in Table 5 for comparison. Note that the hyperfine coupling constants (in Gauss) derived from the EPR spectra differ somewhat, that the assignments by the two groups differ greatly, and that there exists no agreement as to the number of coupling atoms (cf. last row in Table 5).

The largest measured hyperfine coupling constant of ≈11.5 G was assigned to N1, and this value agrees closely with the a_{N1} values computed for **2** and **3**. The computations show that the absolute values of the hyperfine coupling constants of the amino-N and of the amino-H atoms are small (<1 G) and that they are certainly nowhere close to 3 G. Because of this finding and considering the discussion of the geometries and of the electronic structures of **2** and **3**, we confidently conclude that the amino group is not responsible for the hyperfine structure

dx.doi.org/10.1021/tx2005458 | Chem. Res. Toxicol. 2012, 25, 620−633

Table 5. Isotropic Hyperfine Coupling Constants of ^{14}N and ^{1}H Atoms in Radicals 2 and 3[a]

QCI//DFT, 2		QCI//DFT, 3		Anderson et al.		Lloyd et al.	
N1	12.02	N1	12.49	N	11.65	N1	11.50
N2	2.14	N2	−1.82	N^{γ}	3.62	N2	3.38
$N(NH_2)$	−0.25	$N(NH_2)$	0.45	N^{δ}	2.98	$N(NH_2)$	2.98
H(C5)	−4.75	H(C5)	−2.38	(Ar)H, 2	3.05	(Ar)H, 2	3.53
H(C6)	−0.67	H(C6)	−0.17				
H(C7)	−3.04	H(C7)	−2.19				
H(C8)	−3.23	H(C8)	−0.57				
$(H_2N)H_a$	−0.37	$(H_2N)H_a$	−0.28			NH_2, 2	2.95
$(H_2N)H_b$	−0.37	$(H_2N)H_b$	0.75				
N4	4.05	N4	3.47				
6 (>1.5)		5 (>1.5)		5		7	

[a]All values are in Gauss. The number of nuclei with a > 1.5 G is given in the last row.

of the experimental EPR spectra. Instead, theory shows large hyperfine coupling constants for N4 and for several aryl-H atoms.

CONCLUSIONS

TPZ chemistry involves large systems with variable extended conjugation and near-degeneracies, opportunities for N-pyramidalization within the triazene, closed-shell systems with low-lying spin-polarized excited states, and complicated patterns of spin delocalization and spin polarization. The theoretical study of this chemistry is nontrivial, it is anything but routine, and it relies on intertemporal choices. We present results obtained with hybrid density functional theory, second-order and higher-order perturbation theory, and quadratic configuration interaction theory. Theoretical level dependencies occur, some are drastic, others are more subtle, and we do not hide such issues. Overall, the QCI//DFT and QCI//MP2 data give qualitatively similar results, we tend to favor QCI//DFT over QCI//MP2 results, and we are confident that our conclusions will survive improvements of the theoretical approach.

The doublet radicals **2**, **3**, and **4** are heavily spin-polarized radicals (Σ_α < 1.4 and Σ_β > −0.4). The *N*,*N*-dioxide **1** and the *N*-oxides **5** and **6** have closed-shell singlet ground states and low-lying, singlet biradical (**SP-1**, **SP-6**) or biradicaloid (**SP-5**) excited states. Most of the spin density of the doublet radicals **2**, **3**, and **4** is located in one (N,O)-region with modest delocalization into the benzene ring (Σ_1 > 0.9). Significant amounts of spin density occur in both rings in the singlet biradical(oid) excited states of **1**, **5**, and **6**.

TPZ carries an amino group at C3 (X = NH_2) and a variety of analogues have been studied in which this amino group was replaced by other groups (X = H, CH_3, Ph, OMe, ...) based on the notion that X might help stabilize spin density at C3. Our results show, however, that **3** and **4** are not C3-centered radicals and that, instead, high spin densities occur in the (N1,O)-region of **3** and in the (N4,O)-region of **4**, respectively. In the case of **3**, the spin density analysis supports and corroborates the LDRMP-radical notation originally suggested by Lloyd et al.[6]

There is no doubt that the variation of the C3-substituent X affects the outcome of the reduction/protonation sequence **1** → **2** → **3** and/or **4** in significant ways. If X does not affect this chemistry through its radical-stabilizing ability, then one must conclude that X affects the electron density at C3 and the molecular polarity. The dipole moment of the N2−C3(X) bond is very large, and the nature of X provides a powerful handle to modulate the N2−C3 bond polarity with opposite effects on the two NO regions.

Our studies show that **3** is clearly not a C3-centered radical but a (N1,O)-region centered radical. The pK_a(**3**) = 6 was reported based on the observation of the disproportionation reaction of **3** to **5** and **1**. Our studies show very low proton affinities of radical anion **2** and suggest that the pK_a of radical [**2**+H] might even be lower than 6. Considering the result of the spin density analysis and pK_a([**2**+H] ≤ 6, it is nontrivial and perhaps problematic to assume that spin traps (such as PBN) would form adducts by addition to C3 of **3**. In fact, in neutral or basic solution, one should expect [**2**]/[**3**] ≫ 1, and EPR measurements should report on radical anion **2** and its spin trap adducts. Comprehensive experimental studies are needed of the structures and hyperfine coupling constants of these spin trap adducts together with theoretical studies of their spin density distributions to make possible the direct comparison of measured (EPR) and computed (spin density distributions) hyperfine coupling constants.

ASSOCIATED CONTENT

Supporting Information

Four tables with the energies and thermochemical parameters computed at the levels B3LYP/6-31G* and QCI/6-31G*//B3LYP/6-31G*, and MP2(full)/6-31G* and QCI//6-31G*//MP2(full)/6-31G*, spin populations and atom and fragment charges computed at the QCI//MP2 level, one figure of spin densities of **1**, **2**, **3a**, and **4b** computed at DFT and MP2 levels, an expanded version of Figure 1, and Cartesian coordinates of all DFT and MP2 optimized structures (28 pages). This material is available free of charge via the Internet at http://pubs.acs.org.

AUTHOR INFORMATION

Corresponding Author

*E-mail: glaserr@missouri.edu (R.G.); gatesk@missouri.edu (K.S.G.).

Author Contributions

R.G. and K.G. designed the study, J.Y. and R.G. conducted the research, and R.G. and J.Y. wrote the article. All authors edited and approved the final manuscript.

Notes

The authors declare no competing financial interest.

■ ABBREVIATIONS

EPR, electron paramagnetic resonance; RHF, restricted Hartree−Fock; ROHF, restricted open-shell Hartree−Fock; UHF, unrestricted Hartree−Fock; PUHF, projected UHF; MPx, Møller−Plesset perturbation theory of x-th order; UMPx, unrestricted MPx theory; PUMPx, projected UMPx; DFT, density functional theory; QCISD, quadratic configuration theory with single and double excitations; RQCISD, restricted QCISD; UQCISD, unrestricted QCISD; DMSO, dimethyl sulfoxide; TPZ, tirapazamine; BTZ, benzotriazinyl; BTO, 1,2,4-benzotriazine 1,4-*N*,*N*-dioxide

■ REFERENCES

(1) (a) Brown, J. M., and Wilson, W. R. (2004) Exploiting tumour hypoxia in cancer treatment. *Nat. Rev. Cancer 4*, 437−447. (b) Brown, J. M. (1999) The hypoxic cell: a target for selective cancer therapy—Eighteenth Bruce F. Cain Memorial Award lecture. *Cancer Res. 59*, 5863−5870. (c) Denny, W. A., and Wilson, W. R. (2000) Tirapazamine: a bioreductive anticancer drug that exploits tumour hypoxia. *Expert Opin. Invest. Drugs 9*, 2889−2901. (d) Vaupel, P., Kallinowski, F., and Okunieff, P. (1989) Blood flow, oxygen and nutrient supply, and metabolic microenvironment of human tumors: a review. *Cancer Res. 49*, 6449−6465. (e) Wilson, W. R. (1992) Tumor Hypoxia: Challenges for Cancer Chemotherapy, iin *The Search for New Anticancer Drugs* (Waring, M. J., and Ponder, B. A. J.., Eds.) Kluwer Academic: Lancaster, PA. (f) Zeman, E. M., Brown, J. M., Lemmon, M. J., Hirst, V. K., and Lee, W. W. (1986) SR-4233: a new bioreductive agent with high selective toxicity for hypoxic mammalian cells. *Int. J. Radiat. Oncol. Biol. Phys. 12*, 1239−1242.

(2) Laderoute, K. (1988) Molecular mechanisms for the hypoxia-dependent activation of 3-amino-1,2,4-benzotriazine-1,4-dioxide (SR 4233). *Biochem. Pharmacol. 37*, 1487−1495.

(3) Laderoute, K. L., Wardman, P., and Rauth, M. (1988) Molecular mechanisms for the hypoxia-dependent activation of 3-amino-1,2,4-benzotriazine-1, 4-dioxide (SR 4233). *Biochem. Pharmacol. 37*, 1487−1495.

(4) Wardman, P., Priyadarsini, K. I., Dennis, M. F., Everett, S. A., Naylor, M. A., Patel, K. B., Stratford, I. J., Stratford, M. R. L., and Tracy, M. (1996) Chemical properties which control selectivity and efficacy of aromatic N-oxide bioreductive drugs. *Br. J. Cancer 74*, S70−S74.

(5) Priyadarsini, K. I., Tracy, M., and Wardman, P. (1996) The one-electron reduction potential of 3-amino-1,2,4-benzotriazine 1,4-dioxide (tirapazamine): a hypoxia-selective bioreductive drug. *Free Radical Res. 25*, 393−399.

(6) Lloyd, R. V., Duling, D. R., Rumyanseva, G. V., Mason., R. P., and Bridson, P. K. (1991) Microsomal reduction of 3-amino-1,2,4-benzotriazine 1,4-dioxide to a free radical. *Mol. Pharmacol. 40*, 440−445.

(7) Patterson, L. H., and Taiwo, F. A. (2000) Electron paramagnetic resonance spectrometry evidence for bioreduction of tirapazamine to oxidising free radicals under anaerobic conditions. *Biochem. Pharmacol. 60*, 1933−1935.

(8) Daniels, J. S., and Gates, K. S. (1996) DNA cleavage by the antitumor agent 3-amino-1,2,4-benzotrizaine 1,4-dioxide (SR4233): evidence for involvement of hydroxyl radical. *J. Chem. Soc 118*, 3380−3385.

(9) Hwang, J. -T., Greenberg, M., Fuchs, T., and Gates, K. S. (1999) of the hypoxia-selective antitumor agent tirapazamine with a C1′-radical in single-stranded and double-stranded DNA: the drug and its metabolites can serve as surrogates for molecular oxygen in radical-mediated DNA damage reactions. *Biochemistry 38*, 14248−14255.

(10) Fuchs, T., Chowdhury, G., Barnes, C. L., and Gates, K. S. (2001) 3-amino-1,2,4-benzotriazine 4-oxide: characterization of a new metabolite arising from bioreductive processing of the antitumor agent 3-amino-1,2,4-benzotrizine 1,4-dioxide (Tirapazamine). *J. Org. Chem. 66*, 107−114.

(11) Kotandeniya, D., Ganley, B., and Gates, K. S. (2002) Oxidative DNA base damage by the antitumor agent 3-amino-1,2,4-benzotriazine 1,4-dioxide (Tirapazamine). *Bioorg. Med. Chem. Lett. 12*, 2325−2329.

(12) Birincioglu, M., Jaruga, P., Chowdhury, G., Rodriguez, H., Dizdaroglu, M., and Gates, K. S. (2003) DNA base damage by the antitumor agent 3-amino-1,2,4-benzotrizine 1,4-dioxide (Tirapazamine). *J. Chem. Soc. 125*, 11607−11615.

(13) Zagorevski, D., Yuan, Y., Fuchs, T., Gates, K. S., Song, M., Breneman, C., and Greenlief, C. M. (2003) A mass spectrometry study of tirapazamine and its metabolites: insights into the mechanism of metabolic transformations and the characterization of reaction intermediates. *J. Am. Soc. Mass Spectrom. 14*, 881−892.

(14) Chowdhury, G., Junnutula, V., Daniels, J. S., Greenberg, M. M., and Gates, K. S. (2007) DNA strand damage product analysis provides evidence that the tumor cell-specific cytotoxin tirapazamine produces hydroxyl radical and acts as a surrogate for O_2. *J. Chem. Soc. 129*, 12870−12877.

(15) Chowdhury, G., Sarkar, U., Pullen, S., Wilson, W. R., Rajapakse, A., Fuchs-Knotts, T., and Gates, K. S. (2012) Strand cleavage by the phenazine di-N-oxide natural product myxin under both aerobic and anaerobic conditions. *Chem. Res. Toxicol. 25*, 197−206.

(16) Anderson, R. F., Shinde, S. S., Hay, M. P., Gamage, S. A., and Denny, W. A. (2003) Activation of 3-amino-1,2,4-benzotriazine 1,4-dioxide antitumor agents to oxidizing species following their one-electron reduction. *J. Chem. Soc. 125*, 748−756.

(17) Shinde, S. S., Hay, M. P., Patterson, A. V., Denny, W. A., and Anderson, R. F. (2009) Spin trapping of radicals other than the ·OH radical upon reduction of the anticancer agent tirapazamine by cytochrome P_{450} reductase. *J. Am. Chem. Soc. 131*, 14220−14221.

(18) Shinde, S. S., Maroz, A., Hay, M. P., Patterson, A. V., Denny, W. A., and Anderson, R. F. (2010) Characterization of radicals formed following enzymatic reduction of 3-substituted analogues of the hypoxia-selective cytotoxin 3-amino-1,2,4-benzotriazine 1,4-dioxide (tirapazamine). *J. Am. Chem. Soc. 132*, 2591−2599.

(19) (a) Li, L.-C., Zha, D., Zhu, Y.-Q., Xu, M.-H., and Wong, N.-B. (2005) Theoretical study of the mechanism of hydroxyl radical release from tirapazamine's undergoing enzymatic catalysis. *Chem. Phys. Lett. 408*, 329−334. (b) Li et al. also studied the reactions of **5** and **6** to 3-amino-1,2,4-benzotriazine by another reduction/protonation/homolysis sequence.

(20) (a) Pogozelski, W. K., McNeese, T. J., and Tullius, T. D. (1995) What species is responsible for strand scission in the reaction of [Fe(EDTA)]2$^-$ and H_2O_2 with DNA? *J. Am. Chem. Soc. 117*, 6428−6433. (b) Pratviel, G., Bernadou, J., and Meunier, B. (1995) Carbon—hydrogen bonds of DNA sugar units as targets for chemical nucleases and drugs. *Angew. Chem., Int. Ed. Engl. 34*, 746−769. (c) Evans, M. D., Dizdaroglu, M., and Cooke, M. S. (2004) Oxidative DNA damage and disease: induction, repair and significance. *Mutat. Res. 567*, 1−61.

(21) Laderoute, K. R., and Rauth, A. M. (1986) Identification of two major reduction products of the hypoxic cell toxin 3-amino-1,2,4-benzotriazine-1,4-dioxide. *Biochem. Pharmacol. 35*, 3417−3420.

(22) Yin, J., Glaser, R., and Gates, K. S. (2012) On the Reaction mechanism of Tirapazamine reduction chemistry: unimolecular N−OH homolysis. Step-wise dehydration or triazene ring-opening. *Chem. Res. Toxicol.*, DOI: 10.1021/tx200546u.

(23) Frisch, M. J., Trucks, G. W., Schlegel, H. B., Scuseria, G. E., Robb, M. A., Cheeseman, J. R., Scalmani, G., Barone, V., Mennucci, B., Petersson, G. A., Nakatsuji, H., Caricato, M., Li, X., Hratchian, H. P., Izmaylov, A. F., Bloino, J., Zheng, G., Sonnenberg, J. L., Hada, M., Ehara, M., Toyota, K., Fukuda, R., Hasegawa, J., Ishida, M., Nakajima, T., Honda, Y., Kitao, O., Nakai, H., Vreven, T., Montgomery, J. A., Jr., Peralta, J. E., Ogliaro, F., Bearpark, M., Heyd, J. J., Brothers, E., Kudin, K. N., Staroverov, V. N., Kobayashi, R., Normand, J., Raghavachari, K., Rendell, A., Burant, J. C., Iyengar, S. S., Tomasi, J., Cossi, M., Rega, N., Millam, J. M., Klene, M., Knox, J. E., Cross, J. B., Bakken, V., Adamo, C., Jaramillo, J., Gomperts, R., Stratmann, R. E., Yazyev, O., Austin, A. J., Cammi, R., Pomelli, C., Ochterski, J. W., Martin, R. L., Morokuma, K., Zakrzewski, V. G., Voth, G. A., Salvador, P., Dannenberg, J. J., Dapprich, S., Daniels, A. D., Farkas, O., Foresman, J. B., Ortiz, J. V.,

Cioslowski, J., and Fox, D. J. (2009) *Gaussian 09*, revision B.01, Gaussian, Inc., Wallingford, CT.
(24) Becke, A. D. (1993) Density-functional thermochemistry. III. The role of exact exchange. *J. Chem. Phys. 98*, 5648−5652.
(25) (a) Pople, J. A. (1999) Nobel lecture: Quantum chemical models. *Rev. Mod. Phys. 71*, 1267−1274. (b) Binkley, J. S., and Pople, J. A. (1975) Møller-Plesset theory for atomic ground-state energies. *Int. J. Quantum Chem. 9*, 229−236.
(26) He., Z., Kraka, E., and Cremer, D. (1996) Application of quadratic CI with singles, doubles, and triples (QCISDT): an attractive alternative to CCSDT. *Int. J. Quantum Chem. 57*, 157−172.
(27) Glaser, R., and Choy, G. S.-C. (1993) Electron and spin density analysis of spin-projected unrestricted Hartree-Fock density matrixes of radicals. *J. Phys. Chem. 97*, 3188−3198.
(28) Sui, Y., Glaser, R., Sarkar, U., and Gates, K. (2007) Stabilities and spin distributions of benzannulated benzyl radicals. *J. Chem. Theory Comput. 3*, 1091−1099.
(29) Glaser, R., Sui, Y., Sarkar, U., and Gates, K. (2008) Electronic structures and spin topologies of γ-picoliniumyl radicals. A study of the homolysis of *N*-methyl-γ-picolinium and of benzo-, dibenzo-, and naphthoannulated analogs. *J. Phys. Chem. A 112*, 4800−4814.
(30) Sholl, D., and Steckel, J. A. (2009) *Density Functional Theory: A Practical Introduction*, Wiley-Interscience, New York, NY.
(31) He, Y., and Cremer, D. (2000) Spin projected coupled-cluster theory with single and double excitations. *Theo. Chim. Acta 105*, 132−144.
(32) Schlegel, H. B., and McDouall, J. J. (1991) Do You Have SCF Stability and Convergence Problems? in *Computational Advances in Organic Chemistry* (Ögretir, C., and Csizmadia, I. G., Eds.) pp 167−185, Kluwer Academic, The Netherlands.
(33) (a) Chan, W.-T., and Hamilton, I. P. (2003) Mechanisms for the ozonolysis of ethene and propene: reliability of quantum chemical predictions. *J. Chem. Phys. 118*, 1688−1701. (b) Pulay, P., and Liu, R. F. (1990) Methods for finding unrestricted Hartree-Fock solutions and multiple solutions. *J. Phys. Chem. 94*, 5548−5551. (c) Raghavachari, K., Trucks, G. W., Pople, J. A., and Replogle, E. (1989) Highly correlated systems: structure, binding energy and harmonic vibrational frequencies of ozone. *Chem. Phys. Lett. 158*, 207−212.
(34) (a) Kuz'mitskii., V. A. (2004) Instability of the molecular structure of monobenzoporphin to the alternation of the macrocycle bond lengths and its manifestation in the electronic spectra. *J. Appl. Spectrosc. 71*, 777−787. (b) Colvin, M. E., Janssen, C. L., Seidl, E. T., Nielsen, I. M. B., and Melius, C. F. (1998) Energies, resonance and UHF instabilities in polycyclic aromatic hydrocarbons and linear polyenes. *Chem. Phys. Lett. 287*, 537−541.
(35) (a) Sheka, E. F., and Chernozatonskii, L. A. (2010) Broken symmetry approach and chemical susceptibility of carbon nanotubes. *Intl. J. Quant. Chem 110*, 1466−1480. (b) Sheka, E. F. (2007) Chemical susceptibility of fullerenes in view of Hartree-Fock approach. *Intl. J. Quant. Chem. 107*, 2803−2816.
(36) Glaser, R., and Prugger, K. (2012) Iodine Bonding Stabilizes Iodomethane in MIDAS Pesticide. Theoretical Study of Intermolecular Interactions between Iodomethane and Chloropicrin. *J. Agri. Food Chem. 60*, 1776−1787.
(37) Palafox, M. A., Gill, M., Nunez, N. J., Rastogi, V. K., Mittal, L., and Sharma, R. (2005) Scaling factors for the prediction of vibrational spectra. II. The aniline molecule and several derivatives. *Int. J. Quantum Chem 103*, 394−421. (b) Campanelli, A. R., Domenicano, A., and Ramondo, F. (2003) Electronegativity, Resonance, and Steric Effects and the Structure of Monosubstituted Benzene Rings: An ab Initio MO Study. *J. Phys. Chem. 107*, 6429−6440. (c) Tzeng, W. B., Narayanan, K., Shieh, K. C., and Tung, C. C. (1998) A study of the structures and vibrations of $C_6H_5NH_2$, C_6H_5NHD, $C_6H_5ND_2$, $C_6D_5NH_2$, C_6D_5NHD and $C_6D_5ND_2$ in the S1 state by ab initio calculations. *J. Mol. Struct. 428*, 231−240.
(38) Tomasi, J., Mennucci, B., and Cammi, R. (2005) Quantum mechanical continuum salvation models. *Chem. Rev. 105*, 2999−3093.
(39) (a) Swart, M., and Bickelhaupt, F. M. (2006) Proton affinities of anionic bases: trends across the periodic table, structural effects, and DFT validation. *J. Chem. Theory Comput. 2*, 281−287. (b) Del Bene, J. E. (1993) Proton affinities of NH_3, H_2O, and HF and their anions: a quest for the basis-set limit using the dunning augmented correlation-consistent basis sets. *J. Phys. Chem. 97*, 107−110.
(40) Edgecomb, K., and Boyd, R. J. L. (1984) Molecular orbital treatment of substituent effects. 111. Proton affinities of some methyl and carboxylate anions. *Can. J. Chem. 62*, 2887−2891.
(41) Kazazic, S., Kazazic, S., Klasinc, L., McGlynn, S. P., and Pryor, W. A. (2002) Proton affinities of N-O anions and their protonated forms. *J. Phys. Org. Chem. 15*, 728−731.
(42) One should replace pK_a(**3**) by pK_a([**2**+H] to leave open the option for tautomers.
(43) (a) Hwang, J.-T., Greenberg, M. M., Fuchs, T., and Gates, K. S. (1999) Reaction of the hypoxia-selective antitumor agent tirapazamine with a C1′-radical in single-stranded and double-stranded DNA: The drug and its metabolites can serve as surrogates for molecular oxygen in radical-mediated DNA-damage reactions. *Biochemistry 38*, 14248−14255. (b) Daniels, J. S., Gates, K. S., Tronche, C., and Greenberg, M. M. (1998) Direct evidence for bimodal DNA damage induced by tirapazamine. *Chem. Res. Toxicol. 11*, 1254−1257.
(44) Hay, M. P., Gamage, S. A., Kovacs, M. S., Pruijn, F. B., Anderson, R. F., Patterson, A. V., Wilson, W. R., Brown, J. M., and Denny, W. A. (2003) Structure-activity relationships of 1,2,4-benzotriazine 1,4-dioxides as hypoxia-selective analogues of tirapazamine. *J. Med. Chem. 46*, 169−182.
(45) Zeman, E. M., Baker, M. A., Lemmon, M. J., Pearson, B. A., Adams, J. A., Brown, J. M., Lee, W. W., and Tracy, M. (1989) Structure-activity relationships for benzotriazine di-N-oxides. *Int. J. Radiat. Oncol. Biol. Phys. 16*, 977−981.